Harmonic control in electrical drives for transport systems

Thanh Lich Nguyen[1], Van Trang Phung[2]
[1]Department of Mechatronics, Faculty of Mechanical Engineering, University of Transport and Communications, Hanoi, Vietnam
[2]Modelling and Simulation Center, Viettel High Technology Industries Corporation, Hanoi, Vietnam

Article Info	ABSTRACT
	Field-oriented control (FOC) is the most widely used method for controlling alternating current (AC) drives, using Clarke and Park transformations to enable current controllers to manipulate the amplitude of the fundamental component of the phase currents. The inherent advantage of the FOC method is that it transforms current control tasks into a DC domain, thereby enhancing the dynamics of current response and the capability of tracking the current reference. The idea of the FOC can be extended beyond the fundamental component to control some of the harmonics buried in any signals presented in electrical drives, which is particularly critical in transport systems. This paper presents a harmonic control framework, optimized for transport applications, with three different topologies: adaptive linear neural (Adaline), resonant controller (RC), and harmonic controller (HC). The study provides a comprehensive theoretical analysis of the mathematical relationships between these three control structures. Additionally, it explores the application of harmonic controllers in both current and speed control loops. Simulation and experimental results are used to validate the proposed framework, demonstrating its potential to improve the performance of electric drives in vehicles, including enhanced energy efficiency, reduced electromagnetic interference, and smoother torque production.

Corresponding Author:

Thanh Lich Nguyen
Department of Mechatronics, Faculty of Mechanical Engineering
University of Transport and Communications
No. 3 Cau Giay Street, Hanoi, Vietnam
Email: lichnt@utc.edu.vn

1. INTRODUCTION

To address the global challenge of reducing carbon dioxide emissions, electrical machines are widely used in important industrial sectors, particularly in transportation applications such as aerospace, robotics, crane systems, and electric vehicles [1]. Electrical drives are a preferred choice due to their high power density, low maintenance costs, high torque density, and high efficiency [2]. Despite the numerous benefits of electrical drives, there are some unwanted phenomena that lead to torque/speed ripples during the commissioning of electrical machines, affecting their performance and reliability [3]. The most well-known factors contributing to torque ripples are the current measurement error [4], [5], dead-time effects [6], [7], cogging torque harmonics [8], [9], and flux harmonics [10].

Among the above phenomena, the current measurement error is a major source of the periodic disturbances in electrical drives. The DC offset errors in the current measurement result in periodic errors in the q-component of the phase current in the rotor flux-oriented coordinate, hence causing periodic torque ripples [11]. Dead-time insertion, implemented to prevent short circuits in the switches of the voltage source inverters, introduces the sixth-order harmonic and its multiples into the dq-current components [6], [12], [13]. The undesirable harmonics in the modulated voltage distort the output voltage, leading to corresponding

harmonics in the phase currents and subsequently causing ripples in the electromagnetic torque. Additionally, flux harmonics are due to the non-ideal sinusoidal flux distribution in the air gap, which is influenced by the machine construction and the properties of the permanent magnets [14].

In addition to the current ripples, speed oscillations caused by external disturbances can also be observed in electrical drives. This phenomenon is particularly prevalent in transport systems such as conveyor belts and cargo robots, where the mechanical systems attached to the driving machines are characterized by repetitive phenomena. A characteristic feature of such systems is the periodic load torque, which eventually causes speed oscillations. These oscillations introduce undesired harmonics into the control signals, negatively impacting the overall performance. Specifically, they can reduce the precision of the position control loop, decrease the torque per ampere ratio of the electrical machine, and increase the ohmic losses due to the skin effect associated with high-frequency components in the flux and stator current spectra.

To mitigate the negative effects of undesirable harmonics, the implementation of harmonic controllers in industrial electrical drives is crucial [4], [15], [16]. Various harmonic controller topologies have been developed, including the resonant controller (RC) [17], [18], harmonic controller (HC) [19], and adaptive linear neural (Adaline) [15], [20], [21]. The three aforementioned topologies share a common working principle of dealing with the specific harmonic in physical quantities. However, a comprehensive analysis of their similarities and differences, particularly with respect to mathematical description and experimental implementation, is still lacking. This research work focuses on filling this research gap by highlighting the same mathematical description of these topologies and also investigating the differences regarding the discretized implementation and phase compensation techniques.

The main contributions of this work are as follows. First, it demonstrates that while the mathematical descriptions of the three considered topologies are equivalent, their discretized implementations differ due to variations in discretization methods. Second, a novel phase compensation approach is proposed for the Adaline and HC topologies, filling a gap in the existing literature. Third, the effectiveness of the harmonic controllers is validated through both simulation and experimental results, specifically in the context of harmonic cancellation in speed and current control loops.

The remainder of the paper is organized as section 2 is dedicated to the control topologies of Adaline, RC, and HC, followed by the simulation and experimental validation given in section 3. Finally, the conclusions are summarized in section 4.

2. COMPARISON AND IMPLEMENTATION OF HARMONIC CONTROLLERS
2.1. Comparison between Adaline, RC, and HC

To illustrate the similarities between the Adaline, harmonic controller, and the resonant controller, let's consider an example of phase current harmonic control in the rotor flux-oriented reference frame (dq-reference frame). First, the transfer function of the RC will be presented. Then the comparison among the Adaline, HC, and RC will be addressed as follows: i) the HC and RC are compared in terms of mathematical representation and ii) the HC and Adaline are compared with regard to working principle and implementation.

Figure 1(a) shows the structure of the harmonic controller, composed of a resonant component (RC) working in parallel with a conventional proportional-integral (PI) controller [4]. The transfer function of the resonant controller without phase compensation is given by (1).

$$G_{\mathrm{RC}}(s) = K_{\mathrm{i}} \cdot \frac{s}{s^2 + \omega_x^2} \tag{1}$$

Where $\omega_x = 2\pi f_x$ with f_x is the frequency of the xth harmonic to be considered; K_{i} is the gain of the RC; and $G_x(s) = 1/(L_x s + R_x)$ is the equivalent transfer function that combines the transfer functions of the machine, the inverter and the low-pass filter used for the current measurement.

The primary idea of the RC is to provide infinite gain of the open loop at the resonant frequency, and hence it ensures a zero error for the closed control loop. However, the RC controller given in (1) cannot manipulate a resonant frequency that is relatively high compared to the sampling frequency of the control algorithm. This is due to the time delay originated from the control algorithm. The time delay reduces the phase margin of the closed control loop, which is then prone to instability. To address this issue, phase compensation is commonly applied to the RC to increase the phase margin. The transfer function of the modified resonant controller with phase compensation is given in (2) [18], [22].

$$G_{\mathrm{RC}}(s) = K_{\mathrm{i}} \cdot \frac{s \cdot \cos\varphi_{\mathrm{m}} - \omega_x \cdot \sin\varphi_{\mathrm{m}}}{s^2 + \omega_x^2} \tag{2}$$

Where φ_{m} is the compensated phase.

Figure 1(b) depicts the closed-loop current control incorporating the modified resonant controller. As expressed in (2), the transfer function $G_{RC}(s)$ involves two key design parameters, namely the gain K_i and the phase φ_m. Phase compensation is excluded in the scope of this study and will be presented in detail in the ongoing work. Regarding the design of gain K_i, there are some remarks. Firstly, K_i decides the dynamics of the closed loop pertaining to reference tracking capability. The higher the value of K_i, the faster of the output response, but the controller reaches saturation earlier. Secondly, the higher the value of the amplitude associated with the resonant harmonic, the higher the gain K_i. Thirdly, if there are several resonant components, the gains must be optimized sequentially to ensure that the interaction between the harmonic components is under fully taken into account.
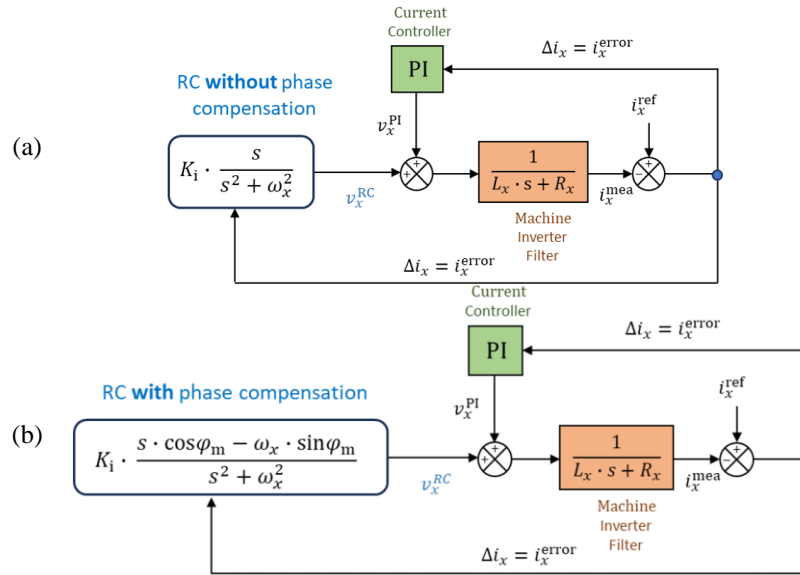

Figure 1. Resonant controller for the current control loop: (a) without phase compensation and (b) with phase compensation

2.1.1. Comparison of HC and RC

This section presents a detailed mathematical analysis demonstrating the equivalence between the resonant controller and the harmonic controller in terms of their mathematical formulation. It is well known that as (3)-(5).

$$x_{cos}(t) = x(t) \cdot \cos(\omega_x t + \varphi_m) = x(t) \cdot \frac{e^{j(\omega_x t + \varphi_m)} + e^{-j(\omega_x t + \varphi_m)}}{2} \tag{3}$$

$$x_{sin}(t) = x(t) \cdot \sin(\omega_x t + \varphi_m) = x(t) \cdot \frac{e^{j(\omega_x t + \varphi_m)} - e^{-j(\omega_x t + \varphi_m)}}{2j} \tag{4}$$

$$\mathcal{L}\{e^{at} f(t)\} \rightarrow F(s - a) \tag{5}$$

Where $\mathcal{L}$ is the Laplace transform and ω_x is the angular velocity of the xth harmonic. Taking the Laplace transformation, we have (6) and (7).

$$X_{cos}(\omega) = \frac{1}{2}[X(\omega - \omega_0) \cdot e^{j\varphi_m} + X(\omega + \omega_0) \cdot e^{-j\varphi_m}] \tag{6}$$

$$X_{sin}(\omega) = \frac{j}{2}[X(\omega - \omega_0) \cdot e^{j\varphi_m} - X(\omega + \omega_0) \cdot e^{-j\varphi_m}] \tag{7}$$

We denote $*$ as the convolution multiplication, then as (8).

$$v_x^{Har}(t) = \{[\Delta i(t) \cdot \cos(\omega_x t) * h(t)]\} \cdot \cos(\omega_x t + \varphi_m) + \{[\Delta i(t) \cdot \sin(\omega_x t) * h(t)]\}$$
$$\cdot \sin(\omega_x t + \varphi_m) \tag{8}$$

We denote as (9) and (10).

$$f_1(t) = \Delta i(t) \cdot \cos(\omega_x t) * h(t) \tag{9}$$

$$f_2(t) = \Delta i(t) \cdot \sin(\omega_x t) * h(t) \tag{10}$$

Then the Laplace transformation of $f_1(t)$ and $f_2(t)$ are as (11) and (12).

$$\begin{aligned}
F_1(s) &= \mathcal{L}\{\Delta i(t) \cdot \cos(\omega_x t) * h(t)\} = \mathcal{L}\{\Delta i(t) \cdot \cos(\omega_x t)\} \cdot H(s) \\
&= \frac{1}{2}[\Delta I(s + j\omega_x) + \Delta I(s - j\omega_x)] \cdot H(s)
\end{aligned} \tag{11}$$

$$\begin{aligned}
F_2(s) &= \mathcal{L}\{\Delta i(t) \cdot \sin(\omega_x t) * h(t)\} = \mathcal{L}\{\Delta i(t) \cdot \sin(\omega_x t)\} \cdot H(s) \\
&= \frac{j}{2}[\Delta I(s + j\omega_x) - \Delta I(s - j\omega_x)] \cdot H(s)
\end{aligned} \tag{12}$$

According to (6) and (11), we have (13).

$$\begin{aligned}
A &= \mathcal{L}\{[\Delta i(t) \cdot \cos(\omega_x t) * h(t)] \cdot \cos(\omega_x t + \varphi_m)\} = \mathcal{L}\{f_1(t) \cdot \cos(\omega_x t + \varphi_m)\} \\
&= \frac{1}{2}\{F_1(s - j\omega_x) \cdot e^{j\varphi_m} + F_1(s + j\omega_x) \cdot e^{-j\varphi_m}\} \\
&= \frac{1}{4}\left\{ \begin{matrix} [\Delta I(s) + \Delta I(s - 2j\omega_x)] \cdot H(s - j\omega_x)] \cdot e^{j\varphi_m} \\ +[\Delta I(s + 2j\omega_x) + \Delta I(s)] \cdot H(s + j\omega_x) \cdot e^{-j\varphi_m} \end{matrix} \right\}
\end{aligned} \tag{13}$$

According to (7) and (12), we have (14).

$$\begin{aligned}
B &= \mathcal{L}\{[\Delta i(t) \cdot \sin(\omega_x t) * h(t)] \cdot \sin(\omega_x t + \varphi_m)\} = \mathcal{L}\{f_2(t) \cdot \sin(\omega_x t + \varphi_m)\} \\
&= \frac{j}{2}\{F_2(s - j\omega_x) \cdot e^{j\varphi_m} - F_1(s + j\omega_x) \cdot e^{-j\varphi_m}\} \\
&= \frac{1}{4}\left\{ \begin{matrix} [\Delta I(s) - \Delta I(s - 2j\omega_x)] \cdot H(s - j\omega_x)] \cdot e^{j\varphi_m} \\ -[\Delta I(s + 2j\omega_x) - \Delta I(s)] \cdot H(s + j\omega_x) \cdot e^{-j\varphi_m} \end{matrix} \right\}
\end{aligned} \tag{14}$$

Substitute (13) and (14) into (8) we have (15).

$$\mathcal{L}(v_x^{\text{Har}}) = A + B = \frac{1}{2}\{H(s - j\omega_x) \cdot e^{j\varphi_m} + H(s + j\omega_x) \cdot e^{-j\varphi_m}\}\Delta I(s) \tag{15}$$

From (15) with $H(s) = K_i/s$, the transfer function of the harmonic controller is (16).

$$\begin{aligned}
G_{\text{HC}}(s) &= \frac{1}{2}[H(s - j\omega_x) \cdot e^{j\varphi_m} + H(s + j\omega_x) \cdot e^{-j\varphi_m}] \\
&= \frac{1}{2}\frac{K_i}{s - j\omega_x} \cdot e^{j\varphi_m} + \frac{1}{2}\frac{K_i}{s + j\omega_x} \cdot e^{-j\varphi_m} \\
&= \frac{K_i (s \cdot \cos\varphi_m - \omega_x \cdot \sin\varphi_m)}{s^2 + \omega_x^2}
\end{aligned} \tag{16}$$

From (2) and (16) it is obvious that the transfer functions of the HC and of the RC are identical.

2.1.2. Comparison of HC and Adaline
The graphical depiction of the HC is shown in Figure 2, with (17).

$$\theta_x = \int \omega_x dt \tag{17}$$

Where: θ_x is the electrical angle of the xth harmonic. The relationship between the Adaline and the harmonic controller topologies, as shown in Figures 3(a) and 3(b), is now discussed. The Adaline topology with phase compensation, as depicted in Figure 3(a), is a contribution to this work. In the same manner as the RC, the Adaline with phase compensation enhances the system stability and improves the dynamic performance of the reference tracking.

The (18) and (19) describe the weight update law in the Adaline model, where $w_{x,\text{Ada}}^{\cos}$ and $w_{x,\text{Ada}}^{\sin}$ are weight parameters associated with the xth harmonic at angle θ_x. Specifically, these weights are updated by adding a term proportional to the learning rate η, current error Δi_x, and sine/cosine values of θ_x defined in (17).

$$w_{x,\text{Ada}}^{\cos} = w_{x,\text{Ada}}^{\cos} + \eta \cdot \Delta i_x \cdot \cos(\theta_x) \tag{18}$$

$$w_{x,\mathrm{Ada}}^{\sin} = w_{x,\mathrm{Ada}}^{\sin} + \eta \cdot \Delta i_x \cdot \sin(\theta_x) \tag{19}$$

It is necessary to mention again that for different harmonics corresponding to distinct resonant frequencies the appropriate learning rate must be chosen sequentially to ensure stability and optimal performance. The final estimated harmonic voltage v_x^{Ada} is then incorporated into the current control loop to enhance harmonic compensation.

On the other hand, (20) and (21) define the update law for the HC, where $w_{x,\mathrm{Har}}^{\cos}$ and $w_{x,\mathrm{Har}}^{\sin}$ are obtained through integral operations involving $K_i \cdot \Delta i_x$, and the corresponding trigonometric terms.

$$w_{x,\mathrm{Har}}^{\cos} = \int K_i \cdot \Delta i_x \cdot \cos(\theta_x) \cdot \mathrm{d}t \tag{20}$$

$$w_{x,\mathrm{Har}}^{\sin} = \int K_i \cdot \Delta i_x \cdot \sin(\theta_x) \cdot \mathrm{d}t \tag{21}$$

Where K_i is the gain of the harmonic controller. The selection of K_i can be done by the root-locus method and is conducted one-by-one to consider the interaction between different HCs corresponding to different harmonics [23]. By comparing (18) with (20) and (19) with (21), we observe that if we set $\eta = K_i \cdot \Delta T$, where ΔT is the sampling time of the integral, and if the approximation of the integrals in (20) and (21) adopts the forward Euler method, then we obtain (22) and (23).

$$w_{x,\mathrm{Har}}^{\cos} = w_{x,\mathrm{Har}}^{\cos} + K_i \cdot \Delta i_x \cdot \cos(\theta_x) \cdot \Delta T \tag{22}$$

$$w_{x,\mathrm{Har}}^{\sin} = w_{x,\mathrm{Har}}^{\sin} + K_i \cdot \Delta i_x \cdot \sin(\theta_x) \cdot \Delta T \tag{23}$$

It is observed that the update rules for the Adaline and the HC become mathematically identical. This confirms that the two methods are fundamentally equivalent.
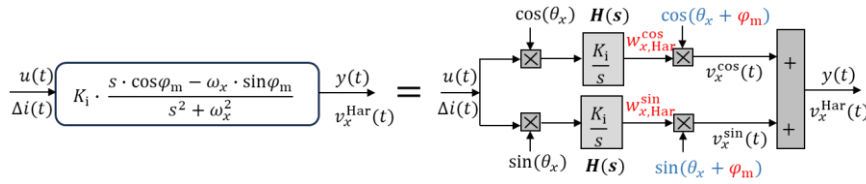

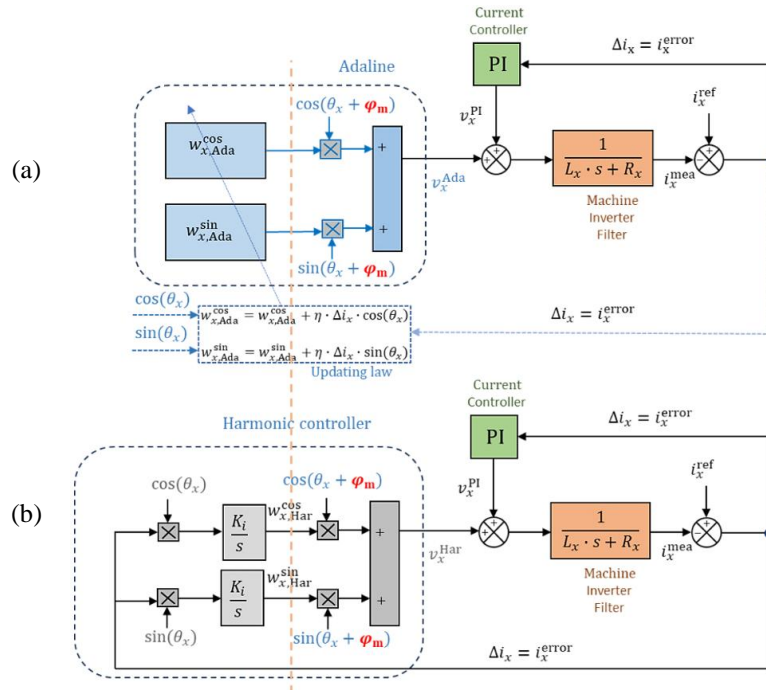Figure 2. Structure of the harmonic controller

Figure 3. Structures of the (a) Adaline and (b) harmonic controllers equipped with a PI controller

There are several important remarks that can be drawn from Adaline and HC. First, both of them operate based on a single-phase transformation that is similar to Park's transformation adopted in field-oriented control (FOC). This transformation allows the update rule to work directly with the DC component of the controlled signal, improving both the dynamics and accuracy of the control algorithm. Both Adaline and HC ensure precise pole placement at the resonant frequency when discretizing the control algorithm with any method.

2.2. Implementation of the harmonic controller

As presented in section 2.1., the Adaline, the RC, and the HC are mathematically equivalent. The differences among these topologies lie in their discretization methods. The discretized poles of the resonant controller, whose topology is shown in Figure 1(a), strongly depend on the discretization method [17]. Ideally, the resonant controller provides infinite gain at $s_{1,2} = \pm j\omega_h$. Consequently, the discretized denominator of the resonant controller should be in the form of (24).

$$\text{Denominator} = (s - s_1)(s - s_2) \rightarrow (z - e^{-j\omega_x T_s})(z - e^{j\omega_x T_s}) = z^2 - 2\cos(\omega_x T_s)z + 1 \quad (24)$$

Where T_s is the sampling time of the harmonic controller. Table 1 summarizes the denominator forms of the resonant controller according to different discretization methods. It is obvious that only the method in group E, consisting of the zero-order hold (ZOH), first-order hold (FOH), Tustin with pre-warping (TP), impulse response (IPM), and zero-pole matching (ZPM), ensures precise poles of the resonant controller after the discretization process. In contrast, other discretization methods introduce pole shifts around the resonant frequency. This shift reduces the gain of the resonant component at the resonant frequency, resulting in a non-zero steady-state error in the closed loop control system.

The determination of the phase compensation plays a crucial role in facilitating the implementation of harmonic controllers. In principle, the compensated phase for each harmonic can be defined by a look-up table. To build up the look-up table, a procedure as depicted in Figure 4 can be employed. The machine operates at different operating points defined by different load torques and speeds using a conventional PI current controller, without implementing RC, HC, or Adaline controllers. At each operating point, the reference and measured current in the d- and q-axes are recorded and processed using an online fast Fourier transform (FFT) algorithm. The main function of the online FFT algorithm is to extract the phase information of the considered harmonics embedded in the reference and measured currents. The phase difference between these signals determines the required phase compensation at each operating point. By combining the phase compensation data from multiple operating points, the final look-up table for the phase compensation is built. For simple implementation, linear interpolation can be used for the look-up table.

Table 1. Discretization of the resonant controller

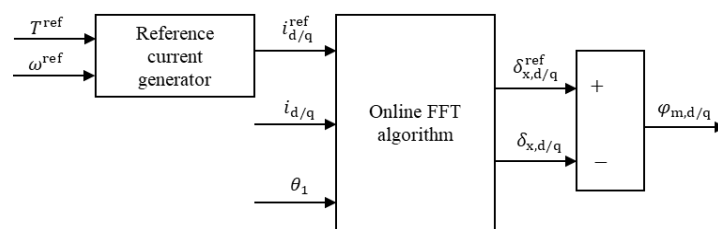| Group	Expression	Denominator
A	$R^f(z)$ - Forward Euler	$1 - 2z^{-1} + z^{-2}(\omega_x^2 T_s^2 + 1)$
B	$R^b(z)$ - Backward Euler	$(\omega_x^2 T_s^2 + 1) - 2z^{-1} + z^{-2}$
C	$R^t(z)$ - Tustin	$(\omega_x^2 T_s^2 + 4) + (2\omega_x^2 T_s^2 - 8)z^{-1} + z^{-2}(\omega_x^2 T_s^2 + 4)$
D	$R^{f\&b}(z)$ - Forward&Backward	$1 + (\omega_x^2 T_s^2 - 2)z^{-1} + z^{-2}$
E	$R^{zoh}(z), R^{foh}(z), R^{tp}(z), R^{ipm}(z), R^{zpm}(z)$	$1 - 2\cos(\omega_x T_s)z^{-1} + z^{-2}$

Figure 4. Procedure for building the look-up table

The three types of controllers are then compared in terms of memory requirement and computational complexity. As already mentioned in section 2.2, the discretization methods belonging to group E ensure an infinite gain of the resonant controller, as given in (2), at the resonant frequency, making them suitable for the RC implementation. For evaluation purposes, the Tustin method with pre-wrapping is selected to assess the runtime performance and memory requirements. The discretized transfer function of the resonant controller is expressed as (25) [24].

$$G_{RC}(s) = K_i \cdot \frac{s \cdot \cos\varphi_m - \omega_x \cdot \sin\varphi_m}{s^2 + \omega_x^2} \rightarrow G_{RC}(z)$$

$$= K_i \cdot \frac{\frac{1}{2}(1-z^{-2})\cos\varphi_m \sin(\omega_x T_s) - (1+2z^{-1}+z^{-2})\sin\varphi_m \sin^2(\frac{\omega_x T_s}{2})}{\omega_m(1-2\cos(\omega_x T_s)z^{-1}+z^{-2})} \tag{25}$$

Where T_s is the sampling time of the RC.

For the case of Adaline and HC, the forward Euler discretization method is adopted due to its simplicity, while still ensuring good behavior of the controllers. It is necessary to mention that the single precision floating-point variable is preferred in the automotive industry due to the compromise between the precision and memory/runtime optimization. Table 2 shows a comparative evaluation of the memory requirement and computational load of the RC, HC, and Adaline controllers. It is observed that the execution of HC and Adaline is identical and less complicated compared to the RC. In addition, an optimized trigonometric function evaluation method, such as those presented in [25], can be used to reduce the runtime of the 04 trigonometric functions, making the three proposed controllers feasible in reality.

Table 2. Memory requirement and computational burden of the RC, HC, and Adaline

Method	RC	HC	Adaline
Memory requirement	5 singles	3 singles	3 singles
Load burden	+ 04 trigonometric functions: $\cos\varphi_m$, $\sin\varphi_m$, $\sin(\omega_x T_s)$, $\cos(\omega_x T_s)$. + 16 multiplications + 06 additions or subtractions + 01 division	+ 04 trigonometric functions: $\cos\theta_x$, $\sin\theta_x$, $\cos(\theta_x + \varphi_m)$, $\sin(\theta_x + \varphi_m)$ + 08 multiplications + 04 additions or subtractions	+ 04 trigonometric functions: $\cos\theta_x$, $\sin\theta_x$, $\cos(\theta_x + \varphi_m)$, $\sin(\theta_x + \varphi_m)$ + 08 multiplications + 04 additions or subtractions

3. SIMULATION AND EXPERIMENTAL VALIDATION

In this section, simulation and experimental results are used to verify the effectiveness of the current and harmonic controllers in an electrical drive.

3.1. Simulation validation for harmonic current controller

The parameters of the current control loop are defined as follows: $R_x = 90 \text{ m}\Omega$, $L_x = 1 \text{ mH}$, $f_s = 10 \text{ kHz}$, $f_x = 600 \text{ Hz}$, $\varphi_m = 1.5 \text{ rad}$. The amplitude of the current reference is set to 4 A. The simulations are conducted using the HC, Adaline, and RC controllers, both with and without phase compensation. Additionally, the operation performance of the RC controller is evaluated under different discretization methods.

Figures 5(a)-5(c) illustrate the current response behavior of the HC, Adaline, and RC controllers, respectively, demonstrating their ability to effectively track the reference current within approximately 0.1 s. The magnified view of these three controllers, as shown in Figures 6(a)-6(c), highlights a zero current tracking error, illustrating the excellent reference tracking performance of the harmonic controller.
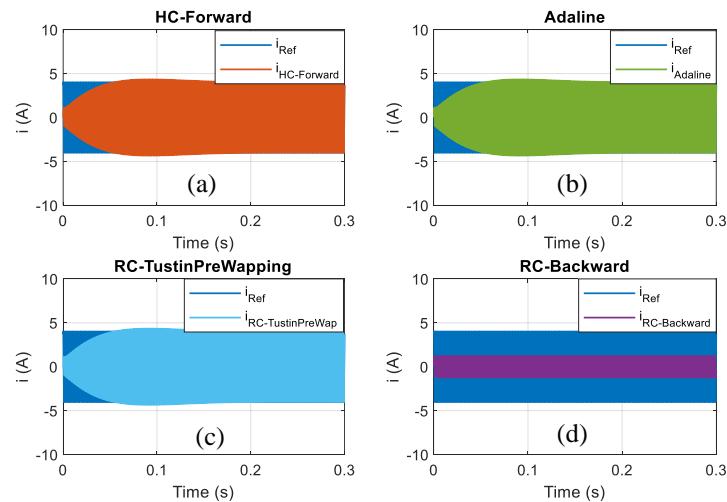

Figure 5. (Simulation) of current responses of (a) HC, (b) Adaline, (c) RC, and (d) RC-backward with phase compensation

In contrast, Figure 5(d) and its enlarged view in Figure 6(d) show the performance of the RC controller when a discretization method from Group B in Table 1 is employed. In this scenario, the current error persists over time, indicating that the RC controller cannot achieve accurate current regulation under this discretization approach. Notably, as depicted in Figure 5(c), the RC controller maintains proper functionality only when discretization methods categorized under Group E are employed. These results are consistent with the theoretical analysis outlined in section 2.1, reinforcing the critical role of discretization selection in ensuring optimal controller performance.

Figures 7(a)-7(d) and its magnified view in Figures 8(a)-8(d) show the current responses without the phase compensation for the harmonic component. In this case, the current response becomes unstable as it goes to infinity within a short time. This phenomenon proves that phase compensation is mandatory for the harmonic controller, especially when the controlled signal frequency is relatively high compared to the sampling frequency.
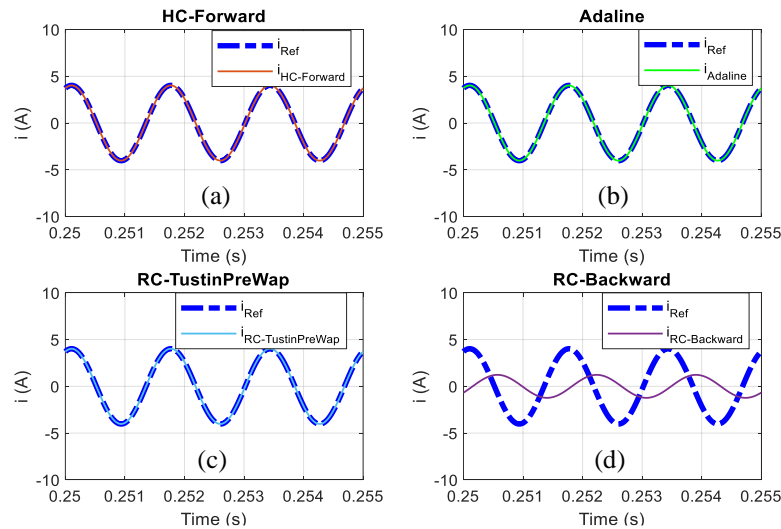

Figure 6. Zoom-in of (simulation) current responses of (a) HC, (b) Adaline, (c) RC, and (d) RC-backward with phase compensation
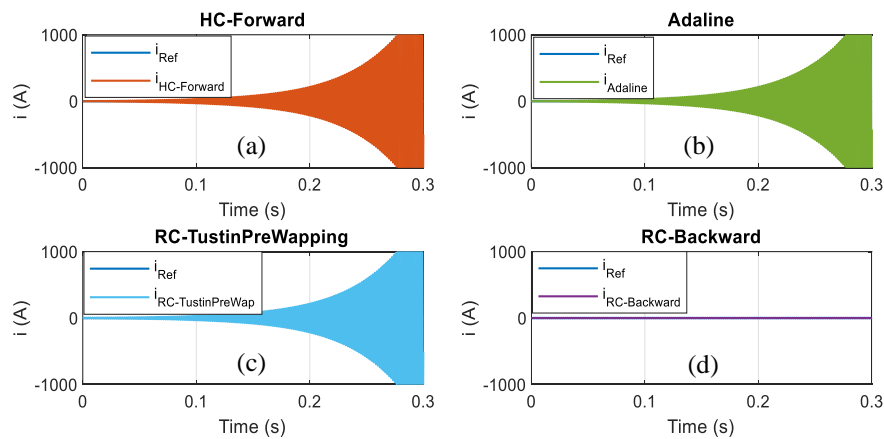

Figure 7. (Simulation) current responses of (a) HC, (b) Adaline, (c) RC, and (d) RC-backward without phase compensation

3.2. Experimental validation of harmonic speed controller for the PMSM

In this section, experimental results are presented to verify the effectiveness of the proposed harmonic speed control for a permanent magnet synchronous machine (PMSM). The control scheme for the PMSM, as shown in Figures 9(a) and 9(b), is based on the parameters given in Table 3. The PMSM is equipped with a slider-crank mechanism, where the load torque varies periodically as a function of the crank angle. A detailed description of the mechanical configuration and the angle-dependent load torque can be found in [26]. The

slider-crank mechanism is an example of repetitive mechanical systems commonly encountered in transportation applications, such as crane systems, cargo robots, and conveyor belts. The field-oriented control (FOC) algorithm is implemented on a dSPACE 1104 board with a sampling frequency of 5 kHz. The current control loops are designed to achieve a bandwidth of 400 Hz, ensuring precise control performance. For feedback, a 2048-pulse, 4-fold encoder is employed to measure the true angle of the rotor, which is used as a reference value for the control system. This experimental setup facilitates accurate evaluation of the proposed control strategies under practical operating conditions.
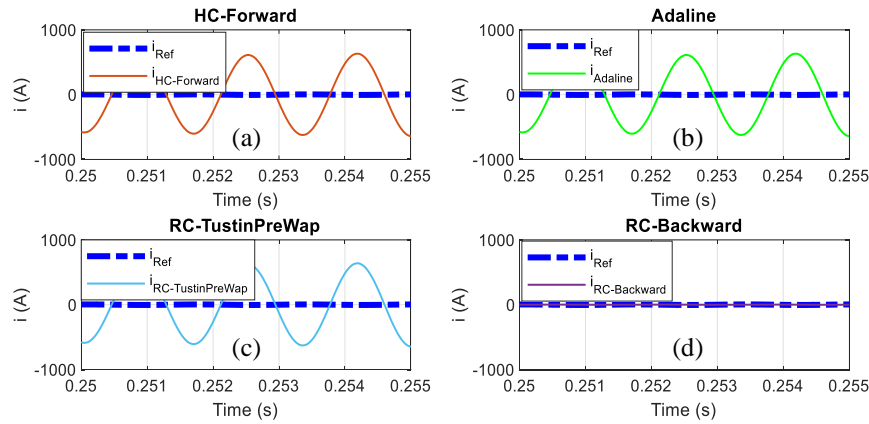

Figure 8. Zoom-in of (simulation) current responses of (a) HC, (b) Adaline, (c) RC, and (d) RC-backward without phase compensation
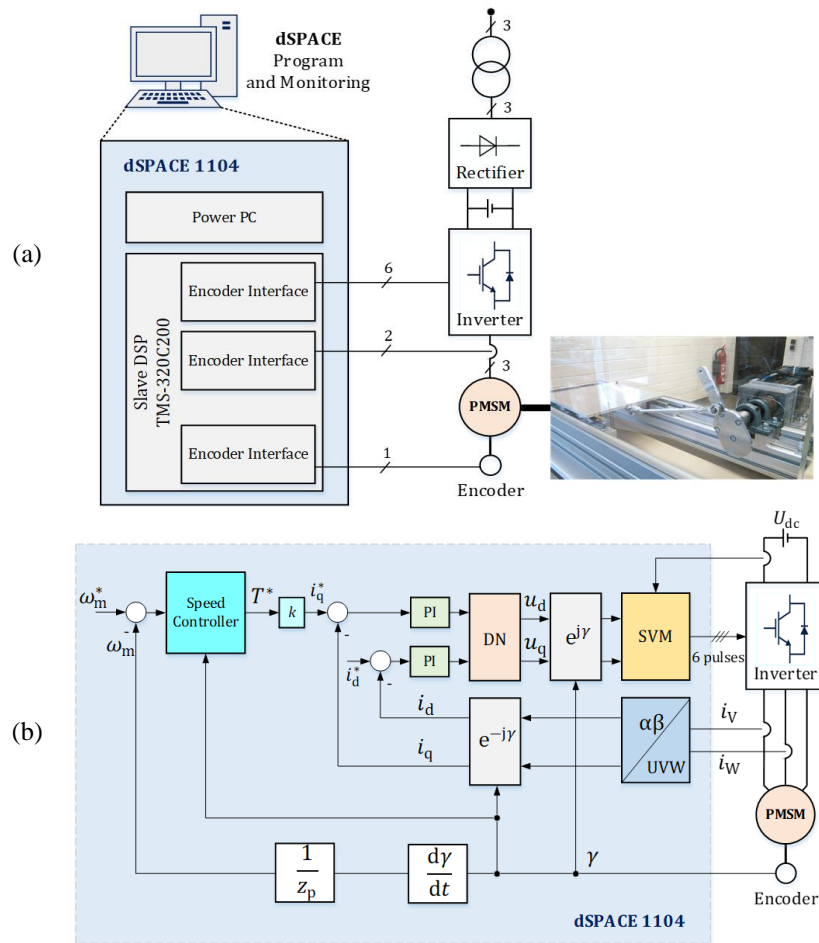

Figure 9. The PMSM is installed in a slider-crank mechanism: (a) hardware connection and (b) control scheme

The periodic nature of the load torque introduces speed ripples that cannot be effectively suppressed by a conventional proportional-integral (PI) speed controller. To overcome this limitation, a harmonic controller is used in this work to mitigate the speed oscillations. It is important to note that the slider crank mechanism is directly attached to the shaft of the driving machine, hence, the system should be operated at low speeds to prevent excessive vibration in the mechanism. The proposed harmonic controller is designed to actively compensate for harmonics up to the 5th order of the speed, ensuring smoother and more stable operation of the system.

Figure 10 shows the speed response of the system when controlled by the conventional PI controller and the HC. In this case, the reference speed was set to 80 min^{-1} with a slope of 60 min^{-1}/s. The reason for using of a ramp-up reference speed rather than a step one is to evaluate the performance of the HC under dynamic conditions. Using a step-reference speed would likely cause the speed controller to become saturated during transients, making no difference between the HC and the PI controllers. As the operating frequency, derived from the operating speed, is significantly lower than the sampling frequency, phase compensation is not mandatory for the harmonic controller. It can be clearly observed in Figure 10 that the HC ensures better reference tracking capability of the speed control loop in both dynamic and steady state modes. In the test bench for a mechatronic system equipped with a slider-crank mechanism, the load torque varies periodically, completing one cycle per one revolution of the rotor. The changing load torque results in a speed oscillation of 16 min^{-1} (20% of the reference speed) when using the conventional PI controller. In contrast, the HC effectively eliminates the speed oscillation, especially in the steady state. This improvement is further illustrated through the spectrum analysis of the speed error, defined as the deviation between the reference speed and the actual response, as shown in Figure 11 for both the PI and HC controllers. It is realized that the HC significantly reduces the harmonics in the speed response, demonstrating its effectiveness in achieving a ripple-free operation.

Figure 12 presents the experimental speed response of the system using Adaline (black) and RC (blue) controllers. Both controllers achieve the target speed of 90 rpm with a rise time of approximately 1 second. The Adaline controller responds promptly following its reference (gray), with slight steady-state oscillations. The RC controller tracks its delayed reference step at 2.8 seconds with high accuracy and minimal overshoot. Both controllers demonstrate effective tracking, with Adaline showing a faster initial response and RC offering high steady-state accuracy.

Table 3. Parameters of the PMSM

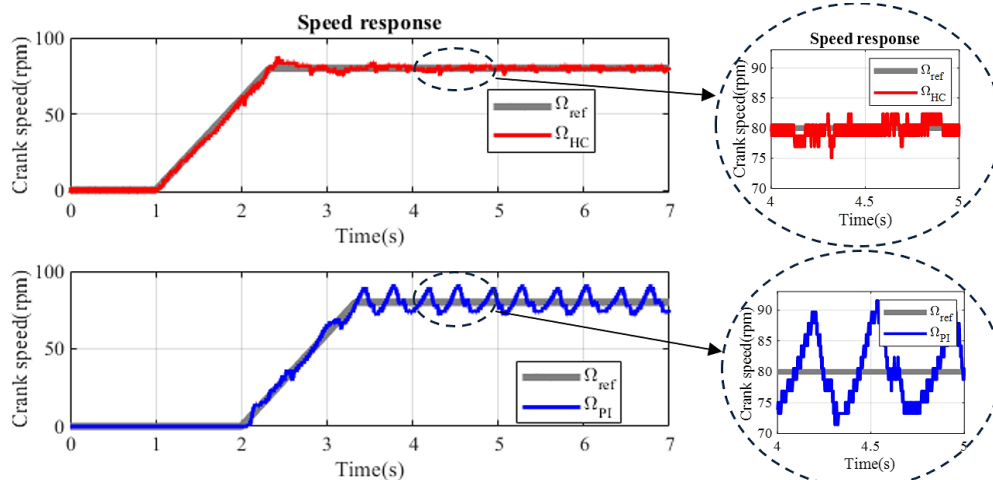| Parameters	Value	Unit
Machine model	ABB SDM 101-005N8-115	
Nominal power	1.54	kW
Nominal voltage	360	V
Nominal velocity	3000	min^{-1}
Nominal torque	4.9	Nm
Pole pairs	3	
Winding resistance R_{UV}	6.4	Ω
Winding inductance L_{UV}	21.8	mH
Moment of inertia	0.0006	$kg \cdot m^2$

Figure 10. (Experiment) speed responses with the HC (red) and conventional PI speed controller (blue)
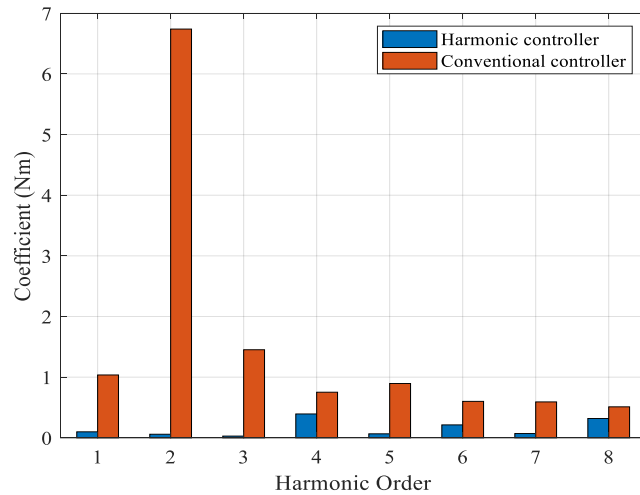
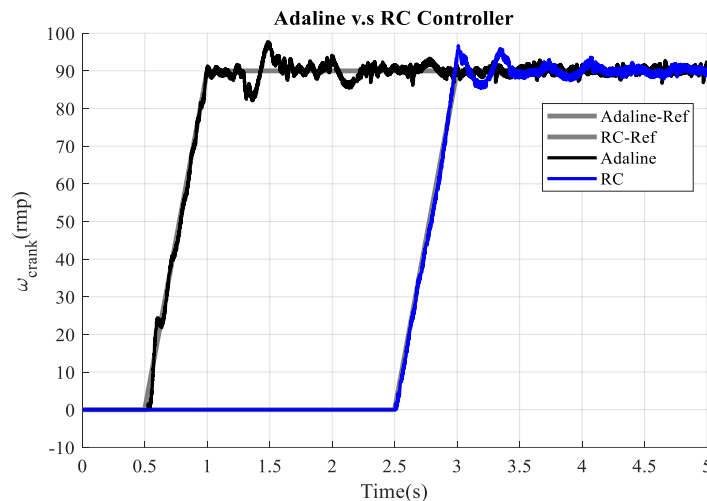Figure 11. (Experiment) spectrum of speed error: (blue) with the HC controller, (red) with conventional PI controller

Figure 12. (Experiment) speed response with the Adaline (black) and RC (blue) controllers

4. CONCLUSION

This paper has successfully demonstrated the mathematical relationship between the Adaline, the harmonic controller and the RC controllers. Although the three topologies shared an identical mathematical description, their digital implementation might be different depending on the discretization method used. For the Adaline and HC, which inherently include sine/cosine operations in their topologies, any discretization method can be applied to the integral term without compromising functionality. However, in the case of the RC, specific discretization methods must be carefully chosen to ensure proper operation. Experimental validation confirms that the RC, HC, and Adaline are effective in mitigating harmonics buried in the phase current and speed of electrical drives. This functionality is highly essential for transport applications, where accurate harmonic control improves energy efficiency, minimizes electromagnetic interference, and ensures smoother torque generation, which are key factors in the reliable and sustainable operation of electric and hybrid vehicles. In addition, from a software maintenance perspective, the Adaline and HC offer practical benefits due to their simpler and more flexible implementation, making them more favorable for long-term deployment in advanced transport systems. By overcoming the challenges associated with harmonic mitigation, the proposed methods establish a framework for enhancing the efficiency and reliability of electric drive systems, thus contributing significantly to the advancement of sustainable transport technologies

AUTHOR CONTRIBUTIONS STATEMENT
This journal uses the Contributor Roles Taxonomy (CRediT) to recognize individual author contributions, reduce authorship disputes, and facilitate collaboration.

Name of Author	C	M	So	Va	Fo	I	R	D	O	E	Vi	Su	P	Fu
Thanh Lich Nguyen	✓	✓	✓		✓	✓	✓	✓	✓	✓		✓	✓	✓
Van Trang Phung	✓		✓	✓		✓	✓		✓	✓	✓	✓		

C : **C**onceptualization	I : **I**nvestigation	Vi : **Vi**sualization
M : **M**ethodology	R : **R**esources	Su : **Su**pervision
So : **So**ftware	D : **D**ata Curation	P : **P**roject administration
Va : **Va**lidation	O : Writing - **O**riginal Draft	Fu : **Fu**nding acquisition
Fo : **Fo**rmal analysis	E : Writing - Review & **E**diting	

CONFLICT OF INTEREST STATEMENT
Authors state no conflict of interest.

INFORMED CONSENT
We have obtained informed consent from all individuals included in this study.

DATA AVAILABILITY
The data that support the findings of this study are available from the corresponding author, [TLN], upon reasonable request.

REFERENCES
[1]   C. Liu, "emerging electric machines and drives - An overview," *IEEE Transactions on Energy Conversion*, vol. 33, no. 4, pp. 2270–2280, Oct. 2018, doi: 10.1109/TEC.2018.2852732.

[2]   Z. Song and F. Zhou, "Observer-based predictive vector-resonant current control of permanent magnet synchronous machines," *IEEE Transactions on Power Electronics*, vol. 34, no. 6, pp. 5969–5980, Jun. 2019, doi: 10.1109/TPEL.2018.2870904.

[3]   J. Yang, W.-H. Chen, S. Li, L. Guo, and Y. Yan, "Disturbance/uncertainty estimation and attenuation techniques in PMSM drives—A survey," *IEEE Transactions on Industrial Electronics*, vol. 64, no. 4, pp. 3273–3285, Apr. 2017, doi: 10.1109/TIE.2016.2583412.

[4]   Q. Zhang *et al.*, "An adaptive proportional-integral-resonant controller for speed ripple suppression of PMSM drive due to current measurement error," *International Journal of Electrical Power & Energy Systems*, vol. 129, p. 106866, Jul. 2021, doi: 10.1016/j.ijepes.2021.106866.

[5]   M. Kim, S.-K. Sul, and J. Lee, "Compensation of current measurement error for current-controlled PMSM drives," *IEEE Transactions on Industry Applications*, vol. 50, no. 5, pp. 3365–3373, Sep. 2014, doi: 10.1109/TIA.2014.2301873.

[6]   S.-H. Hwang and J.-M. Kim, "Dead time compensation method for voltage-fed PWM inverter," *IEEE Transactions on energy conversion*, vol. 25, no. 1, pp. 1–10, Mar. 2010, doi: 10.1109/TEC.2009.2031811.

[7]   J.-H. Lee and S.-K. Sul, "Inverter nonlinearity compensation through deadtime effect estimation," *IEEE Transactions on Power Electronics*, vol. 36, no. 9, pp. 10684–10694, Sep. 2021, doi: 10.1109/TPEL.2021.3061285.

[8]   L. Dosiek and P. Pillay, "Cogging torque reduction in permanent magnet machines," *IEEE Trans. Ind. Appl.*, vol. 43, no. 6, pp. 1565–1571, Oct. 2007, doi: 10.1109/TIA.2007.908160.

[9]   L. Dai, S. Niu, W. Zhang, J. Gao, and S. Huang, "Harmonic modeling and ripple suppression of electromagnetic torque in IPMSMs," *IEEE Transactions on Industrial Electronics*, pp. 1–11, 2024, doi: 10.1109/TIE.2024.3384614.

[10] A. Gebregergis, M. H. Chowdhury, M. S. Islam, and T. Sebastian, "Modeling of permanent-magnet synchronous machine including torque ripple effects," *IEEE Transactions on Industry Applications*, vol. 51, no. 1, pp. 232–239, Jan. 2015, doi: 10.1109/TIA.2014.2334733.

[11] M. S. Rafaq and J.-W. Jung, "A Comprehensive review of state-of-the-art parameter estimation techniques for permanent magnet synchronous motors in wide speed range," *IEEE Transactions on Industrial Informatics*, vol. 16, no. 7, Art. no. 7, Jul. 2020, doi: 10.1109/TII.2019.2944413.

[12] A. H. Abosh, Z. Q. Zhu, and Y. Ren, "Reduction of torque and flux ripples in space vector modulation-based direct torque control of asymmetric permanent magnet synchronous machine," *IEEE Transactions on Power Electronics*, vol. 32, no. 4, pp. 2976–2986, Apr. 2017, doi: 10.1109/TPEL.2016.2581026.

[13] T. L Nguyen, "Dead-time compensation for 2-level voltage source inverters based on harmonic current controllers," *Journal of Science and Technology on Information and Communications,* Accessed: May 03, 2024. [Online]. Available: https://jstic.ptit.edu.vn/jstic-ptit/index.php/jstic/article/view/549

[14] J. Liu, H. Li, and Y. Deng, "Torque ripple minimization of PMSM based on robust ILC via adaptive sliding mode control," *IEEE Transactions on Power Electronics*, vol. 33, no. 4, pp. 3655–3671, Apr. 2018, doi: 10.1109/TPEL.2017.2711098.

[15] D. T. Vu, N. K. Nguyen, and E. Semail, "Fault-tolerant control for nonsinusoidal multiphase drives with minimum torque ripple," *IEEE Transactions on Power Electronics*, vol. 37, no. 6, pp. 6290–6304, Jun. 2022, doi: 10.1109/TPEL.2021.3133793.

[16] H. Guzman *et al.*, "Comparative study of predictive and resonant controllers in fault-tolerant five-phase induction motor drives," *IEEE Transactions on Industrial Electronics*, vol. 63, no. 1, Art. no. 1, Jan. 2016, doi: 10.1109/TIE.2015.2418732.

[17] A. G. Yepes, F. D. Freijedo, Ó. Lopez, and J. Doval-Gandoy, "High-performance digital resonant controllers implemented with two integrators," *IEEE Transactions on Power Electronics*, vol. 26, no. 2, Art. no. 2, Feb. 2011, doi: 10.1109/TPEL.2010.2066290.

[18] A. G. Yepes, J. Malvar, A. Vidal, O. López, and J. Doval-Gandoy, "Current harmonics compensation based on multiresonant control in synchronous frames for symmetrical n-phase machines," *IEEE Transactions on Industrial Electronics*, vol. 62, no. 5, Art. no. 5, May 2015, doi: 10.1109/TIE.2014.2365155.

[19] D. Wu and K. Chen, "Frequency-domain analysis of nonlinear active disturbance rejection control via the describing function method," *IEEE Transactions on Industrial Electronics*, vol. 60, no. 9, Art. no. 9, Sep. 2013, doi: 10.1109/TIE.2012.2203777.

[20] K. Liu, Q. Zhang, J. Chen, Z. Q. Zhu, and J. Zhang, "Online Multiparameter Estimation of nonsalient-pole PM synchronous machines with temperature variation tracking," *IEEE Transactions on Industrial Electronics*, vol. 58, no. 5, Art. no. 5, May 2011, doi: 10.1109/TIE.2010.2054055.

[21] D. T. Vu, N. K. Nguyen, E. Semail, and H. Wu, "Adaline-based control schemes for non-sinusoidal multiphase drives–Part I: torque optimization for healthy mode," *Energies*, vol. 14, no. 24, Art. no. 24, Jan. 2021, doi: 10.3390/en14248302.

[22] B. Han, J. S. Lee, and M. Kim, "Repetitive controller with phase-lead compensation for Cuk CCM inverter," *IEEE Transactions on Industrial Electronics*, vol. 65, no. 3, pp. 2356–2367, Mar. 2018, doi: 10.1109/TIE.2017.2739678.

[23] V. T. Phung, H. Al-Badrani, and M. Pacas, "Enhanced speed control of a drive with rejection of periodical disturbances," *IEEE Open Journal of the Industrial Electronics Society*, vol. 3, pp. 551–560, 2022, doi: 10.1109/OJIES.2022.3210173.

[24] K. Zhou, D. Wang, Y. Yang, and F. Blaabjerg, "Periodic control of power electronic converters," in *Institution of Engineering and Technology*. Energy Engineering Series, doi.org/10.1049/PBPO082E.

[25] O. Sahin and C. Eyal, "Optimized trigonometric functions on TI Arm cores," *Application Note*. Texas Instruments Incorporated, 2022.

[26] V. T. Phung and M. Pacas, "Load torque estimation in repetitive mechanical systems by using fourier interpolation," in *PCIM Europe 2016; International Exhibition and Conference for Power Electronics, Intelligent Motion, Renewable Energy and Energy Management*, May 2016, pp. 1–8.

BIOGRAPHIES OF AUTHORS

Thanh Lich Nguyen 🆔 Ⓖ SC ◐ received the B.Eng. degree in electrical engineering from Hanoi University of Science and Technology, Hanoi, Vietnam in 2003 and the M.Eng. degree in automation from Hanoi University of Mining and Geology, Hanoi, Vietnam in 2010, and the Ph.D. degree in electrical engineering from the Technical University of Darmstadt, Darmstadt, Germany in 2019. Currently, he is a lecturer at the University of Transport and Communications. His current research interests include power electronics, electrical drives, mechatronics, automation, renewable energy conversion systems, and microgrids. He can be contacted at email: lichnt@utc.edu.vn.

Van Trang Phung 🆔 Ⓖ SC ◐ was born in Hung Yen, Vietnam, in 1986. He received the bachelor's and M.Sc. degrees in control and automation from the Hanoi University of Science and Technology, Hanoi, Vietnam, in 2009 and 2012, respectively. Under the supervision of Prof. Dr.-Ing. Mario Pacas. He received the Dr.-Ing. degree in electrical engineering from the University of Siegen, Siegen, Germany, in 2017. Since 2019, he has been with Viettel High Technology Corporation, Hanoi, Vietnam, as a Project Manager for vehicle simulation systems, where his key aspect lies in the design of the motion system. His fields of interest are motion control, condition monitoring, and optimization of mechatronic systems. He can be contacted at email: trangtdh2@gmail.com.